



Heat transfer analysis in artificial ground freezing under high seepage: Validation and heatlines visualization



Mahmoud A. Alzoubi^a, Ali Madiseh^b, Ferri P. Hassani^a, Agus P. Sasmito^{a,*}

^a Department of Mining and Materials Engineering, McGill University, 3450 University, Frank Dawson Adams Bldg., Montreal, QC, H3A0E8, Canada

^b Norman B. Keevil Institute of Mining Engineering, 511-6350 Stores Road, Vancouver, BC, V6T 1Z4, Canada

ARTICLE INFO

Keywords:

Artificial ground freezing
Heatlines
Enthalpy-porosity method
Porous media
Seepage

ABSTRACT

The primary goal of artificial ground freezing (AGF) system is to create a hydraulic barrier encircling working areas and stall groundwater seepage. This goal is achieved once a consolidated frozen wall is developed between the freeze pipes. Groundwater flow, however, has an undesirable effect on the formation and the growth rate of the frozen body - high water flow could hamper, totally, the establishment of a merged frozen wall between two freeze pipes. Therefore, it is of great interest to evolve a reliable prediction of the transient response of the ground structure toward the AGF process under high seepage flow conditions. This work interprets the multi-phase heat transfer that accompanying the development of a frozen body between two freeze pipes with and without the presence of the groundwater seepage. A mathematical model has been derived, validated, and implemented to simulate the effect of the coolant's temperature, the spacing between two freeze pipes, and the seepage temperature on the closure time and the shape of the frozen body. The results are presented in terms of temperature fields, phase-change interface, velocity-streamlines, and heatlines. The results indicate that spacing between two pipes and seepage velocity have the highest impact on the closure time and the frozen body width.

1. Introduction

Artificial ground freezing (AGF) is employed in many practical engineering applications, for example, in underground mines [1], tunneling [2,3], and environmental engineering (hazardous waste management) [4–6]. Groundwater seepage may have a strong impact on the AGF process, affecting the development of the frozen body, closure time, and, in specific circumstances, prevent the creation of a close, frozen body between two freeze pipes. Understanding the coupled thermal and hydraulic mechanisms associated with AGF process is crucial in many processes, and is thus of considerable practical and theoretical interest.

A typical AGF system consists of two primary domains: (i) the flow of sub-zero coolant in a network of freeze pipes, and (ii) porous ground structure surrounding the pipes. The heat flow between the adjacent domains occurs through the coupled pipe's wall; this is termed a conjugate problem. The physical processes associated with the conjugate, multi-phase AGF process has been discussed thoroughly in our previous work [7].

The freezing process in the ground is governed by two main mechanisms of energy transfer: conductive heat transfer, and forced-convective heat transfer due to groundwater seepage. Since the first model

elaborated by Sagner and Sayles [8], several studies [9–12] addressed the freezing process by solving the conduction energy equation; thus considering the conduction as the principal mechanism of energy transfer. In the last decade or so, various researches discussed a saturated porous medium subject to groundwater seepage [13–20]. These studies modeled the thermal-hydraulic mechanisms by solving the conservation equation of mass and energy. The effect of the groundwater seepage is formulated as a function of the capillary pressure at the phase-change interface. Huang et al. [14] considered the effect of segregation potential in the formulation of the water seepage, which is a function of the average suction in the freezing interface. Yu et al. and McKenzie et al. and [16,17] modeled the seepage velocity as a function of the water head and the specific yield (the volume of water drained-out from a given porous medium under the forces of gravity), and pressure storativity (the volume of water released from a saturated pore aquifer due to a unit drop in hydraulic head per total volume), respectively. Also, Fowler and Krantz [13] employed the cryostatic suction in the formulation of the groundwater seepage. On the other contrary, in order to model the thermal aspects of the phase-change phenomenon, the latent heat of fusion, in these studies, was added to the specific heat capacity of water; this approach is known as the apparent heat capacity approximation. These approaches, however,

* Corresponding author.

E-mail address: agus.sasmito@mcgill.ca (A.P. Sasmito).

<https://doi.org/10.1016/j.ijthermalsci.2019.02.005>

Received 18 August 2018; Received in revised form 4 February 2019; Accepted 5 February 2019

Available online 16 February 2019

1290-0729/ Crown Copyright © 2019 Published by Elsevier Masson SAS. All rights reserved.

Nomenclature

C_E	Ergun's coefficient [–]
C_m	Mushy constant (5×10^6) [–]
C_0	Empirical coefficient [–]
c_p	Specific heat capacity [J/(kg.K)]
D	Diameter [m]
E	Energy [W/m ²]
h	Specific enthalpy [J/kg]
H	Heat function [W/m]
ΔH	Latent heat of fusion [J/kg]
K	Permeability [m ²]
k	Thermal conductivity [W/(m.K)]
L, ℓ	Length [m]
p	Pressure [Pa]
Pe	Péclet number [–]
q	Heat flux [W/m ²]
S_H	Source term [W/m ³]
T	Temperature [K]
t	Time [s]
\mathbf{u}, u, v	Velocity [m/s]
V	Volume [m ³]

Greek Letter

α	Thermal diffusivity [m ² /s]
γ	Liquid fraction [–]
φ	Porosity [–]
μ	Viscosity [Pa.s]
ρ	Density [kg/m ³]
Θ	Volume averaged quantity [–]
θ	Local quantity [–]
ψ	Stream function [m ² /s]

Subscripts

e	Effective
g	Ground
$init$	Initial
ℓ	Liquid
p	Particle
s	Solid
w	Wall

require careful consideration of the temperature, velocity, and latent heat progression in the freezing interface [21]. Alternatively, other researchers [7,22] implemented the enthalpy-porosity approach proposed by Voller and Prakash [23]. This method represents the phase-change interface as a porous zone; the movement of the freezing interface is governed by a modified Darcy source term in the conservation equation of momentum. The enthalpy-porosity is introduced to simplify the modeling requirements without compromising the accuracy of the results. König-Haagen et al. [24] conducted a comprehensive study to evaluate the corresponding accuracy of the most used macroscopic energy formulations. They concluded that, as a rule of thumb, the enthalpy-porosity formulations are more robust and precise, as compared to the apparent heat capacity approach.

In conductive heat transfer problems, heat-flux lines and isotherms are commonly used as standard techniques to visualize the heat transfer. Yet, once convective heat transfer is introduced, either naturally or forced by a fluid flow, one cannot generate an accurate picture of net energy flow by only monitoring these visualization tools. Instead, Kimura and Bejan [25] introduced a generalized concept that could be used to visualize the transfer of heat by fluid flow in convective heat transfer problems, which could be extended to include phase-change processes. Named as “Heatlines Visualization,” the approach is an attractive option that could be dealt with as the convection counterpart of the heat-flux lines used in conduction problems. To the best of our knowledge, however, limited literature (for example [26–28]) applied this concept to visualize the net energy flow in forced-convective heat transfer problems that include phase-change processes.

To continue the work on mathematical modeling and computation of the artificial ground freezing, the mechanistic model by Alzoubi et al. [7,29] is extended to quantify the impact of the groundwater seepage on the progression of the frozen body; in particular, the effect on the closure time and the shape and thickness of the frozen wall. Within this framework, a study is then carried out to evaluate how key factors - spacing between freeze pipes, seepage velocity, coolant's temperature, and seepage's temperature - affect the performance of AGF process. In essence, the mechanistic model considers the two-phase conservation of mass, momentum, and energy. The results are demonstrated in terms of closure time, temperature fields, phase-change iso-therms, streamlines, and heatlines.

In the following, the model development along with its numerical implementation is described in the first part. A brief discussion of the

model validation is followed in the second part. The results of a parametric study that highlights the influence of the design and operating conditions of an AGF system is then carried out. Finally, conclusions are drawn with emphasis on the impact of various design and operating parameters on the AGF under seepage conditions.

2. Model development

Fig. 1 (a) shows a schematic diagram of an AGF system with parallel freeze pipes configuration. A horizontal cross-section that contains two freeze pipes and the surrounding porous ground structure is considered in this study, as illustrated in Fig. 1(b). In order to reduce the AGF model from a general 3D model to a 2D geometry, which describes a cross-section, the model is limited to a plane in which the groundwater flow and heat transfer in the axial direction (z-direction) are small enough to be neglected as compared to the horizontal directions. In this study, the groundwater is assumed to flow horizontally. Hence, the flow in the axial direction could be safely neglected. Vitel et al. [1,30] studied the ground freezing around vertical freeze pipes. The results showed that the horizontal temperature gradient in the ground is significantly larger than the axial temperature gradient. Therefore, the horizontal heat flux between the freeze pipe and the ground structure is more dominant, as compared to the axial heat flux between ground strata. Further, the freeze pipes in this study are arranged in a uniform parallel configuration. The interaction between each two freeze pipes is assumed to be identical; thus the domain under consideration is set as a 2D symmetry geometry. The dimensions of the computational domain, the thermo-physical properties of the ground, and the initial and boundary conditions are based on Pimental et al. experiment [31,32].

2.1. Governing equations

A mathematical model is developed to study the artificial freezing process within a fully saturated porous medium. The domain comprises a solid matrix containing spaces (pores) filled with one or several water phases. The following discussion intends to describe the mass, momentum, and energy equations that govern the thermal and hydraulic aspects of the AGF process. The local volume averaging approximation is implemented over a representative elementary volume to formulate the conservation equations through which the porous medium is treated as a continuum, as depicted in Fig. 2 (left). Within this volume element,

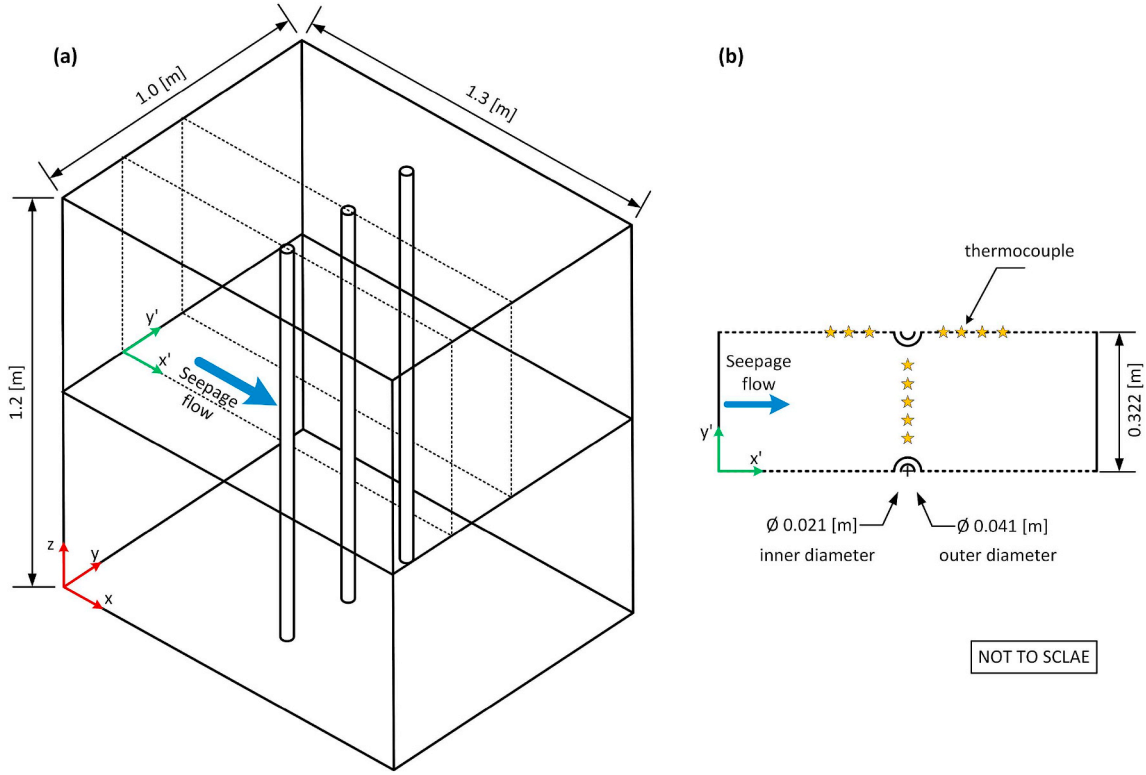


Fig. 1. (a) schematic diagram of Pimentel et al. experiment [32]. (b) Computational domain that includes two freeze pipes.

any local quantity θ is converted into a volume-averaged value Θ using the following expression [33]:

$$\Theta = \frac{1}{V} \int_V \theta dV \quad (1)$$

Also, the pore velocity is defined, based on Dupuit-Forchheimer relationship [34], as ($\mathbf{u} = \varphi \mathbf{u}_\ell$), φ is the porosity, and \mathbf{u}_ℓ is the pore water velocity. The governing equations could be written under the local volume averaging approach as below:

Conservation equation of mass:

$$\frac{\partial}{\partial t}(\rho_\ell) + \nabla \cdot (\rho_\ell \mathbf{u}) = 0 \quad (2)$$

Conservation equation of momentum [23,33]:

$$\frac{1}{\varphi} \frac{\partial}{\partial t}(\rho_\ell \mathbf{u}) + \frac{1}{\varphi^2} [\nabla \cdot (\rho_\ell \mathbf{u} \mathbf{u})] = \frac{1}{\varphi} \nabla \cdot (\mu \nabla \mathbf{u}) - \nabla p - \underbrace{\frac{\mu}{K} \mathbf{u}}_{S_D} - \underbrace{\frac{C_F}{K^{1/2}} \rho_\ell |\mathbf{u}| \mathbf{u}}_{S_F} - \underbrace{\mathbf{u} C_m \frac{(1-\gamma)^2}{\gamma^3}}_{S_m} \quad (3)$$

where S_D , S_F , and S_m are Darcy, Forchheimer, and mushy source terms, respectively.

The Darcy and Forchheimer terms represent the total resistance to the flow. The quadratic Forchheimer's term, S_F , is added for high seepage cases. C_F is a friction factor commonly known as Ergun's coefficient [35]. The soil's permeability K is formulated, based on the semi-empirical Carman-Koseny equation [33], as a function of the porosity φ and the diameter of a soil particle D_p :

$$K = \frac{D_p^2 \varphi^3}{C_0 (1 - \varphi)^2} \quad (4)$$

The empirical coefficient C_0 is usually taken to be a constant and can be adapted for various soil geometries. In this study we consider a value of 180, which is calculated based on the assumption that the ground

structure consists of uniform sized spheres [36].

The last term in Eq. (3), S_m , is a modified Darcy source term that is used to force the superficial velocity, \mathbf{u} , to a value close to zero within the mushy zone. A small constant is generally added to the denominator of the source term to avoid division by zero. C_m is a constant that is based on the morphology of the porous structure. The value of this constant was calibrated from 1×10^5 to 1×10^7 ; the value of 5×10^6 fits best with experimental data, and it is used in this study.

Conservation equation of energy: In this study, the local thermal equilibrium (LTE) hypothesis is implemented. This approach assumes that at any time, t , the temperature difference between the soil particle, groundwater, and ice at pore scale, ℓ_p , is smaller than the global temperature difference at the system scale length. Thus, it is safe to be neglected. The justification behind the LTE assumption has been discussed thoroughly in our previous study [7]. The LTE conservation equation of energy could be written as:

$$\frac{\partial}{\partial t}(\overline{\rho h}) + \nabla \cdot (\rho_\ell h_\ell \mathbf{u}) = \nabla \cdot (k_e \nabla T) - \underbrace{\left[\varphi \rho_\ell \Delta H \frac{\partial \gamma}{\partial t} \right]}_{S_H} + (\nabla \cdot [\rho_\ell \mathbf{u} \gamma \Delta H]) \quad (5)$$

where

$$\overline{\rho h} = \varphi(\gamma \rho_\ell h_\ell + (1 - \gamma) \rho_s h_s) + (1 - \varphi) \rho_p h_p \quad (6)$$

ℓ , s , and p describe the phases: liquid water, solid water (ice), and soil particle, respectively. h stands for the sensible enthalpy of the liquid water. γ is the water fraction. The effective thermal conductivity, k_e , is defined based on the parallel arrangement approach as [33,37]:

$$k_e = \varphi(\gamma k_\ell + (1 - \gamma) k_s) + (1 - \varphi) k_p \quad (7)$$

The source term, S_H , is used to induce the latent heat of fusion, ΔH , during the phase-change process. In the liquid zone, the source term takes a value of zero. Within the mushy zone, the source term increases as the local liquid fraction, γ , decreases from its liquid value of 1 to its solid value of 0. The value of the liquid fraction, γ , could be defined,

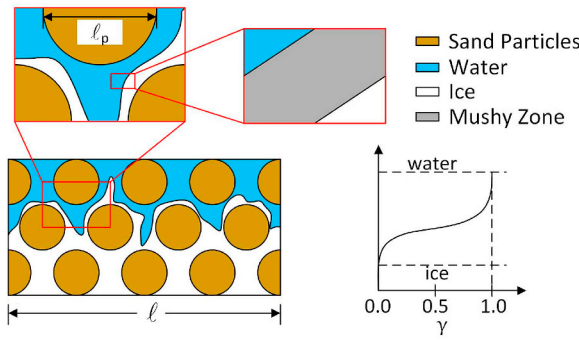


Fig. 2. A schematic of a representative elementary volume (REV) during AGF process, considering the phase-change interface as a mushy zone (left) (after [35]). Possible forms for liquid fraction, γ , within the mushy zone (right) (after [38,41]).

within the mushy zone, as shown in Fig. 2 (right) [38]. The selection of different formulation could influence, to a certain point, the interaction between the solid region and the mushy zone. In this study, a linear formulation is considered

$$\gamma = \frac{T - (T_f - \Delta T)}{2\Delta T} \quad (8)$$

Generally, the temperature range of the mushy zone, $2\Delta T$, during AGF process is significantly small, where $2\Delta T \approx 0.1[^\circ\text{C}]$ [7]. This small value will reduce the influence of liquid fraction formulation on the freezing process. However, in specific cases, such as rock fracture, the temperature range within the mushy zone could reach $6[^\circ\text{C}]$ [30]. In such problems, further examination to select the proper formulation should be considered.

2.2. The concept of heatlines

The concept of the heatlines is evolved, basically, from the use of stream-function and streamlines to visualize the fluid flow. In two-dimensional Cartesian coordinates, one can define the steam-functions as below:

$$\frac{\partial \psi}{\partial y} = u, \quad -\frac{\partial \psi}{\partial x} = v \quad (9)$$

where $\psi(x, y)$ is the stream-function. The flow, by definition, is locally parallel to the constant line of the stream-function, ψ , (i.e., streamlines). Thus, although there is no explicit substitution for the velocity components (u, v) as the source of the local flow attributes, constant streamlines provide a valuable observation of the fluid flow and its characteristics.

Similarly, heat-function and heatlines are introduced as a visualization aid of the transfer of heat by fluid flow. As equation (9) should fulfill the conservation equation of mass, heat-functions should satisfy the conservation equation of energy. Hence, the definition of heat-function could be described as [39]:

$$\frac{\partial H}{\partial y} = E_x, \quad -\frac{\partial H}{\partial x} = E_y \quad (10)$$

where

$$E_x = \left(\rho u [h + \Delta H] - k \frac{\partial T}{\partial x} \right), \quad E_y = \left(\rho v [h + \Delta H] - k \frac{\partial T}{\partial y} \right) \quad (11)$$

E_x and E_y describe the net energy flow in the x-direction and y-direction, respectively. According to this definition, the net energy flow is locally parallel to the heatlines (i.e., $H = \text{constant}$). Therefore, heatlines could be used to describe the actual path of the energy flow.

2.3. Initial and boundary conditions

The initial and boundary conditions of the current mathematical model are defined as below:

- **Initial condition** —Initial temperature and initial velocity at $t = 0$.

$$T_g = T_w = T_{init}, \quad \mathbf{u} = \mathbf{u}_{init} \quad (12)$$

- **Freeze pipes' wall** —Dirichlet boundary conditions for temperature and no-slip conditions.

$$T = T_w, \quad \mathbf{u} = 0 \quad (13)$$

- **Ground (left and right boundaries)** —Neumann boundary condition for temperature in case of no-seepage scenario.

$$\mathbf{n} \cdot \nabla T = 0 \quad (14)$$

Dirichlet boundary for pressure in case of seepage scenario.

$$p = p_{in} \quad (\text{left boundary}) \mid p = p_{out} \quad (\text{right boundary}) \quad (15)$$

- **Ground (top and bottom boundaries)** —Symmetry boundaries (i.e. zero normal velocity, and zero normal gradients of any variable Θ at the symmetry planes.)

$$\mathbf{n} \cdot \mathbf{u} = 0, \quad \mathbf{n} \cdot \nabla \Theta = 0 \quad (16)$$

3. Numerical simulations

The computational domain was developed and meshed using ANSYS software package 16.1. A mesh-sensitivity procedure was performed to ensure the solution's independence. The domain was meshed at the beginning with a coarse mesh consisting of 1×10^3 regular, quad elements, followed by several mesh adaptations until the difference in computed ground's temperature was below 1%. In addition, the influence of the ground's boundaries on the AGF process has been investigated; different widths of the computational domain in the x-direction, ranging from 1 [m] to 100 [m] were implemented, and the ground's temperature at the center between the freeze pipes was compared to ensure a boundary condition independence. For example, in the case of 1.0 [m] space between two freeze pipes, a domain with a width of 11 [m] gave less than 1% deviation compared to the 100 [m] width.

The governing equations along with the initial and the boundary conditions were solved using the finite volume method. The transient coolant temperature (Fig. 3), water and sand thermo-physical properties (Fig. 4 and Table 1), and groundwater seepage were specified and implemented into the numerical model using a user-defined functions

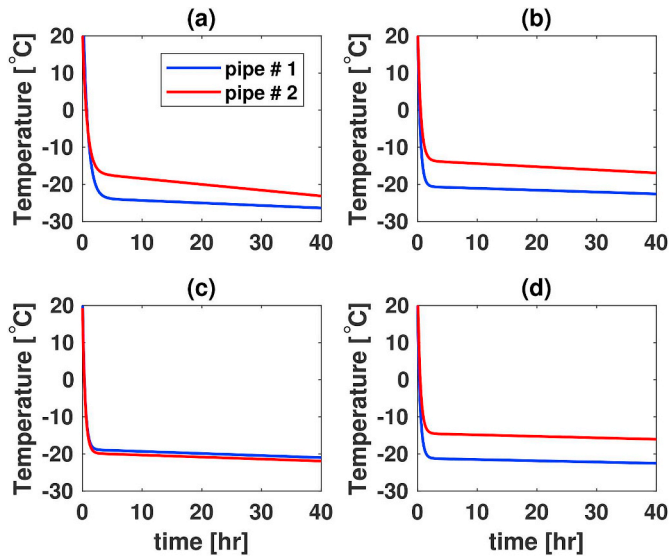


Fig. 3. Wall boundary condition of each freeze pipe under different seepage scenarios: (a) no-seepage; (b) seepage of 1.0 [m/d]; (c) seepage of 1.4 [m/d]; and (d) seepage of 2.0 [m/d] (Adapted from Ref. [32]).

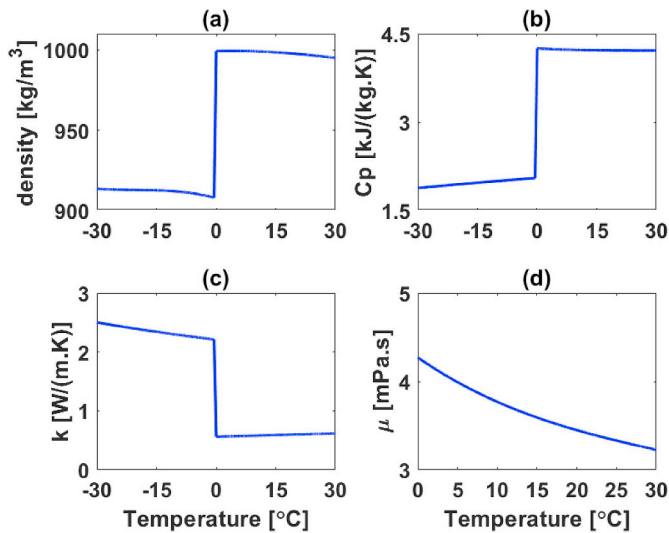


Fig. 4. Water temperature dependent properties: (a) density, (b) specific heat capacity, (c) thermal conductivity, and (d) viscosity.

Table 1
Material properties used in this study.

Properties	Value
Thermal conductivity (sand particle) [W/(m.K)]	4.9
Density (sand particle) [kg/m ³]	2664
Specific heat capacity (sand particle) [J/(kg.K)]	826
Porosity [%]	36
Permeability [m ²]	1.8×10^{-11}
Latent heat of fusion [J/kg]	334000
Water liquidus temperature [°C]	0.1
Water solidus temperature [°C]	0.0

(UDFs). The numerical model was solved with the Semi-Implicit Pressure-Linked Equation (SIMPLE) algorithm and second-order upwind discretization. The convergence criteria were set to 1×10^{-6} for all equations.

4. Model validation

The numerical model is validated against experimental data from Pimentel et al. [31,32] and Sres [40]. They conducted several experiments with and without seepage conditions. The lab-scale setup is characterized by an insulated container with inner dimensions of (1.2 [m] × 1.3 [m] × 1.0 [m]) that contains three vertical freeze pipes with outer diameters of 0.041 [m], as depicted in Fig. 1. In order to simulate the groundwater seepage, two constant-head water tanks have been installed at the opposite faces, perpendicular to the freeze pipes arrangement. More than 70 thermocouples have been installed, at three vertical levels, across one freeze pipes in the x-direction, between two freeze pipes in the y-direction, and at the top and bottom of the freeze pipes' wall. The uncertainties of the thermocouples readings were not explicitly mentioned in the literature [31,32,40]. However, based on the experimental methodology discussed by Pimentel et al. [31,32], we presume that the data is accurate to be used for validation purposes.

The readings of the walls' temperature were curve-fitted, averaged, and used in the model as a transient thermal boundary condition, as shown in Fig. 3. The temperature of the groundwater seepage was set at the initial ground temperature (15 [°C] for the no-seepage case, and 20 [°C] for the other cases). Four scenarios of seepage flow ($v = 0, 1.0, 1.4,$ and 2.0 [m/d]) have been investigated and validated in this study. For the seepage cases, a velocity inlet boundary condition was employed at the beginning. As soon as the hydraulic condition was stabilized, the groundwater inlet was switched into a pressure inlet condition utilizing the corresponding inlet pressure. This shift mimics the actual scenario of an AGF under seepage condition, where the seepage velocity is affected by the reduction of the cross-sectional area between two freeze pipes due to ice growth. The cooling phase started once the hydraulic condition is stabilized. The properties of the materials involved in this study are listed in Table 1. The temperature-dependent properties of water and ice were implemented in the numerical simulation via a UDFs. Good agreement between the model and the experimental data was observed, which can be discerned from Fig. 5.

5. Results and discussion

The results of the validated model are utilized to illustrate the effect of groundwater seepage on the progression of the frozen body at different time stage. The discussion compares the behavior of the heatlines with the behavior of the velocity's streamlines. After that, the framework of the mathematical model is extended to simulate the AGF process with a typical field configuration of parallel freeze pipes. In this study, four key parameters, determining the performance of an AGF process in terms of the thickness and the shape of the frozen body, and closure time, are evaluated with regard to the spacing between two freeze pipes, the velocity of groundwater seepage, brine's temperature, and seepage's temperature, as presented in Table 2.

5.1. Progression of the frozen body

Fig. 6 and Fig. 7 depict the growth of the frozen wall under various seepage scenarios (0, 1.0, 1.4, and 2 [m/day]) at different time stages (1, 5, 20, and 40 [hr]); Fig. 6 describes the temperature contours and the streamlines, while Fig. 7 shows the magnitude of the net energy flow and the heatlines at the same conditions. The results are based on the design and operating parameters of the validated model (see Section 4).

Fig. 6 (a)-(d) describes the temperature contour and the phase-change isotherms at no-seepage condition after 1, 5, 20, and 40 [hr] of freezing, respectively. With no-seepage, the freeze pipes are the primary heat sink, and conductive heat transfer is the main heat transfer mechanism. Therefore, a symmetric frozen body between the freeze pipes is observed in these cases. Correspondingly, the associated heatlines are pointed directly into the freeze pipes, as illustrated in Fig. 7 (a)-(d).

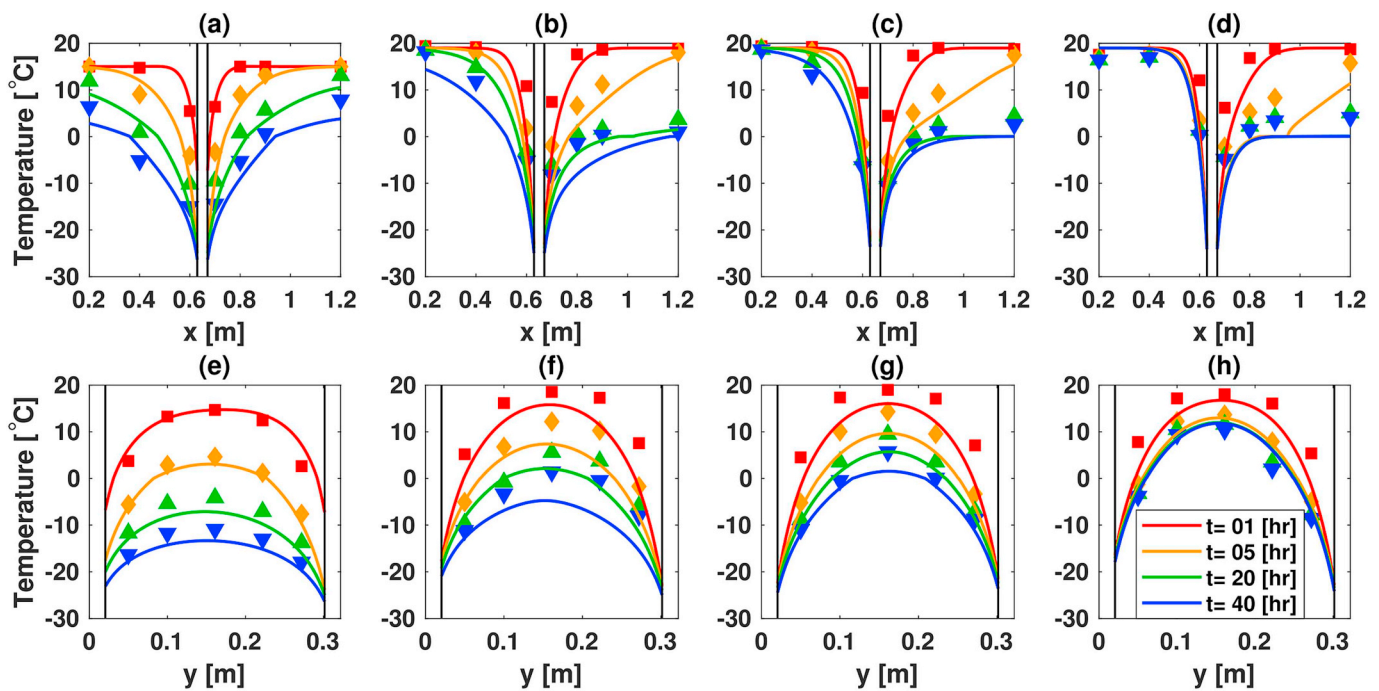


Fig. 5. Model validation against experimental data [31,40] at various seepage. (a), (b), (c), and (d) shows thermocouples in x-direction; whereas (e), (f), (g), and (h) shows thermocouples in y-direction. (a) and (e) no-seepage condition; (b) and (f) seepage of 1.0 [m/d]; (c) and (g) seepage of 1.4 [m/d]; (d) and (h) seepage of 2.0 [m/d].

Table 2

The main parameters at three levels. The base case is highlighted in bold

Spacing	Coolant's Temp.	Seepage Velocity	Seepage Temp.
[m]	[°C]	[m/d]	[°C]
0.3	-20	0.0	5
1.0	-25	0.05	10
2.0	-30	0.1	15

At the beginning of the AGF process, the heat transfer occurs only around the freeze pipes. Thus, the heatlines are only shown in the middle of the domain of interest pointed toward the freeze pipes, as observed in Fig. 7 a. As more heat is extracted from the ground, the size of the frozen body increases and the heatlines start to expand, as shown in Fig. 7 (b). As time advances, the heat extraction reaches the edge of the domain of interest. The energy flows directly toward the freeze pipes, following the path of the heatlines, as shown in Fig. 7 (c) and (d). It is important to recall here that since the main mechanism under the no-seepage condition is conduction, these heatlines represent the heat-flux lines. On the contrary, the overall magnitude of the conduction energy flow is less than 3000 [W/m²]. As we will discuss next, this fact has a direct impact on the growth of the frozen body, especially under high seepage velocity.

Once the seepage is introduced, one expects an immediate interaction between the groundwater flow and the growth of the frozen wall. Yet, after 1 and 5 [hr] of freezing under a seepage velocity of 1 [m/day], the frozen body is barely affected by the flow, as depicted in Fig. 6 (e) and (f), in comparison with Fig. 6 (a) and (b), respectively. On the other hand, Fig. 7 (e) shows a modest bending in the heatlines in the frozen body; at this stage, the effect of the seepage on the ice growth is insignificant, which leads to a symmetric frozen body - similar to the no-seepage case. Originally, before AGF process starts, heatlines flows in parallel with the streamlines, as observed in Figs. 6(e) and Fig. 7 (e). Once freezing begins, the cold pipes start to extract heat from the ground, forcing the heatline to stop and tilt toward the heat sinks. The deflection of the heatlines is clearer after 5 [hr] of freezing, as displayed

in Fig. 7 (f). Additionally, some of the heatlines do not approach the freeze pipes. Instead, they slip away with the direction of the seepage. This phenomena is apparent after 20 [hr] of freezing - the curvature is greater, and more heatlines are escaping the frozen zone in the direction of the flow, as inferred in Fig. 7 (g). It is noticed here that the convective heat transfer increases significantly at this stage, as compared to the previous two stages. This may be attributed to the fact that the seepage has to pass through a narrower passage between the growing, separate frozen bodies, as depicted in Fig. 6 (g). After sufficient time, 40 [hr] in this case, a merged, frozen body is created between the freeze pipes. The convective seepage is not powerful enough to hinder the formation of a closed, frozen wall. However, it is strong enough to cause the frozen wall to swell in the direction of the seepage, as displayed in Fig. 6 (h). Accordingly, the conductive heat transfer becomes the dominant mechanism again while the heat-flux lines draw the direction of the energy flow, as shown in Fig. 7 (h).

The undesirable effect of the groundwater seepage on the evolution of the frozen body increases at higher velocities. The main behavior, however, is similar to low-velocity scenario. The ice growth under 1.4 [m/day] at 1 and 5 [hr] is almost identical to the ice growth under 1 [m/day] at the same time frame, as shown in Fig. 6 (i)-(k), and Fig. 7 (i)-(k), as compared to Fig. 6 (e)-(g), and Fig. 7 (e)-(g), respectively. Several features are apparent from these plots; foremost is that the wall thickness in the 1.0 [m/day] case is larger than the 1.4 [m/day] case. This is due to the fact that the seepage at higher velocity has more convective energy that could interfere with the freeze pipes and reduce their efficiencies. Furthermore, although the 1.4 [m/day] flow suppose to have higher energy, the magnitude of the local net energy flow between the freeze pipes is lower than the 1.0 [m/day], as discerned in Fig. 7 (k) and Fig. 7 (g), respectively. As discussed previously, the narrower the passage between the freeze pipes, the higher the seepage velocity. However, the magnitude of the global net energy flow in the 1.4 [m/day] case is higher, which force the frozen body to elongate more with the flow. Moreover, after 40[hr] of freezing, the frozen body under 1.4 [m/day] seepage stretched more in the direction of the flow and yet to merge, as depicted in Fig. 6 (l) and Fig. 7 (l). The flow convective energy at this stage is still higher than the power of the

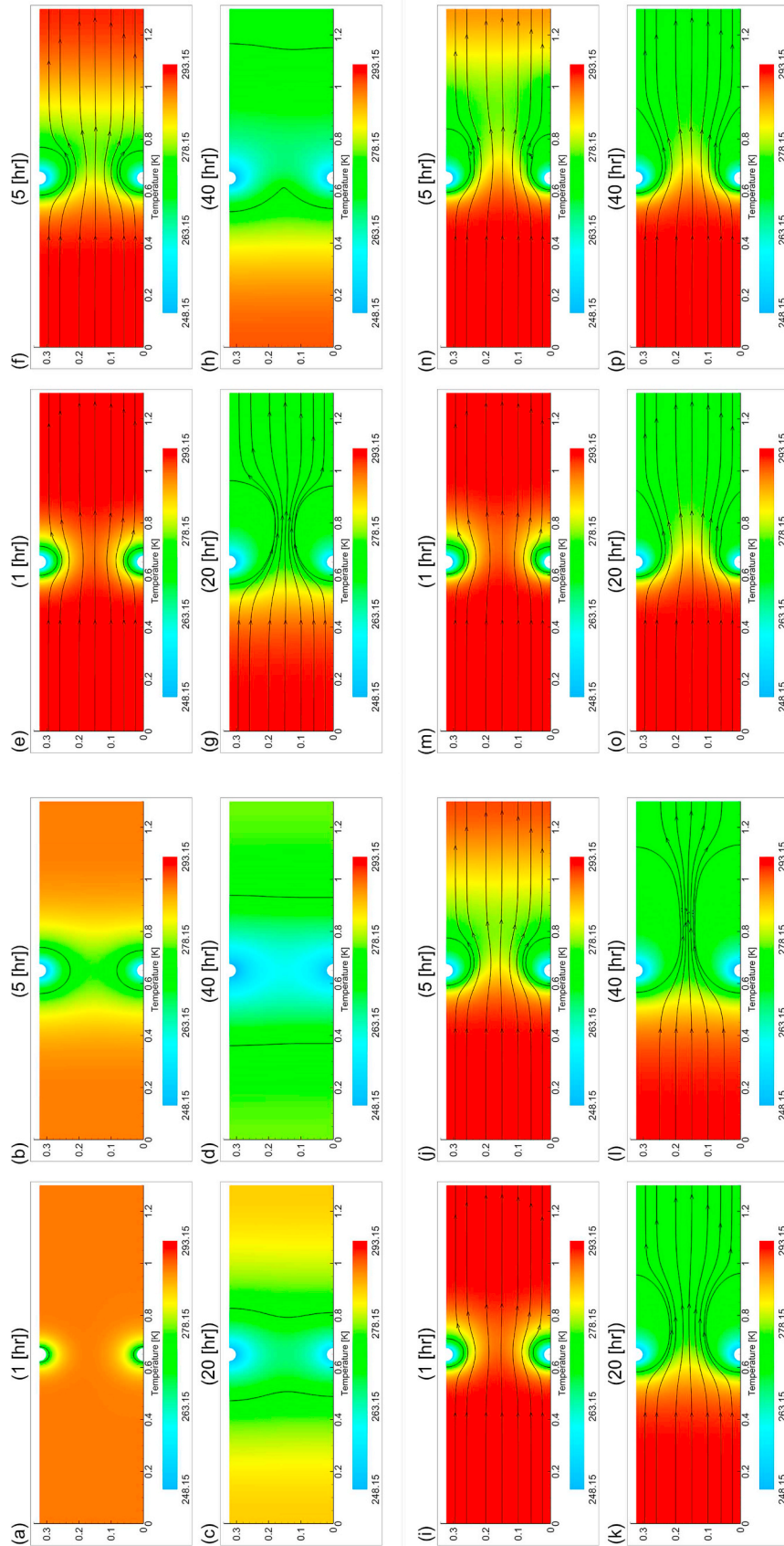


Fig. 6. Temperature fields (contours) and streamlines (lines) of the growth of the frozen body at different time stages and various seepage velocities: (a)–(d) no-seepage condition; (e)–(h) seepage of 1.0 [m/d]; (i)–(l) seepage of 1.4 [m/d]; and (m)–(p) seepage of 2.0 [m/d].

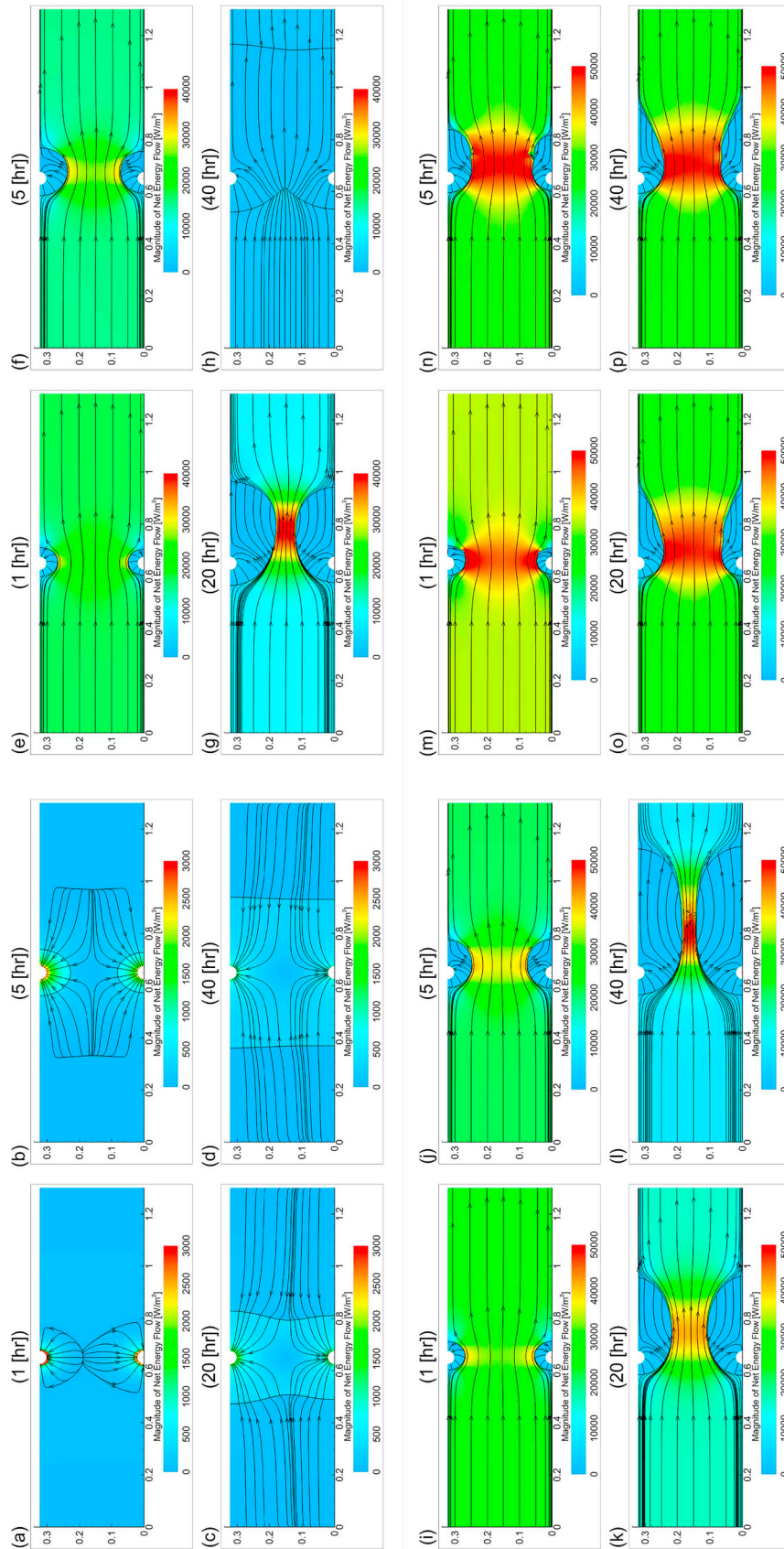


Fig. 7. Magnitude of net energy flow (contours) and heatlines (lines) of the growth of the frozen body at different time stages and various seepage velocities: (a)–(d) no-seepage condition; (e)–(h) seepage of 1.0 [m/d]; (i)–(l) seepage of 1.4 [m/d]; and (m)–(n) seepage of 2.0 [m/d].

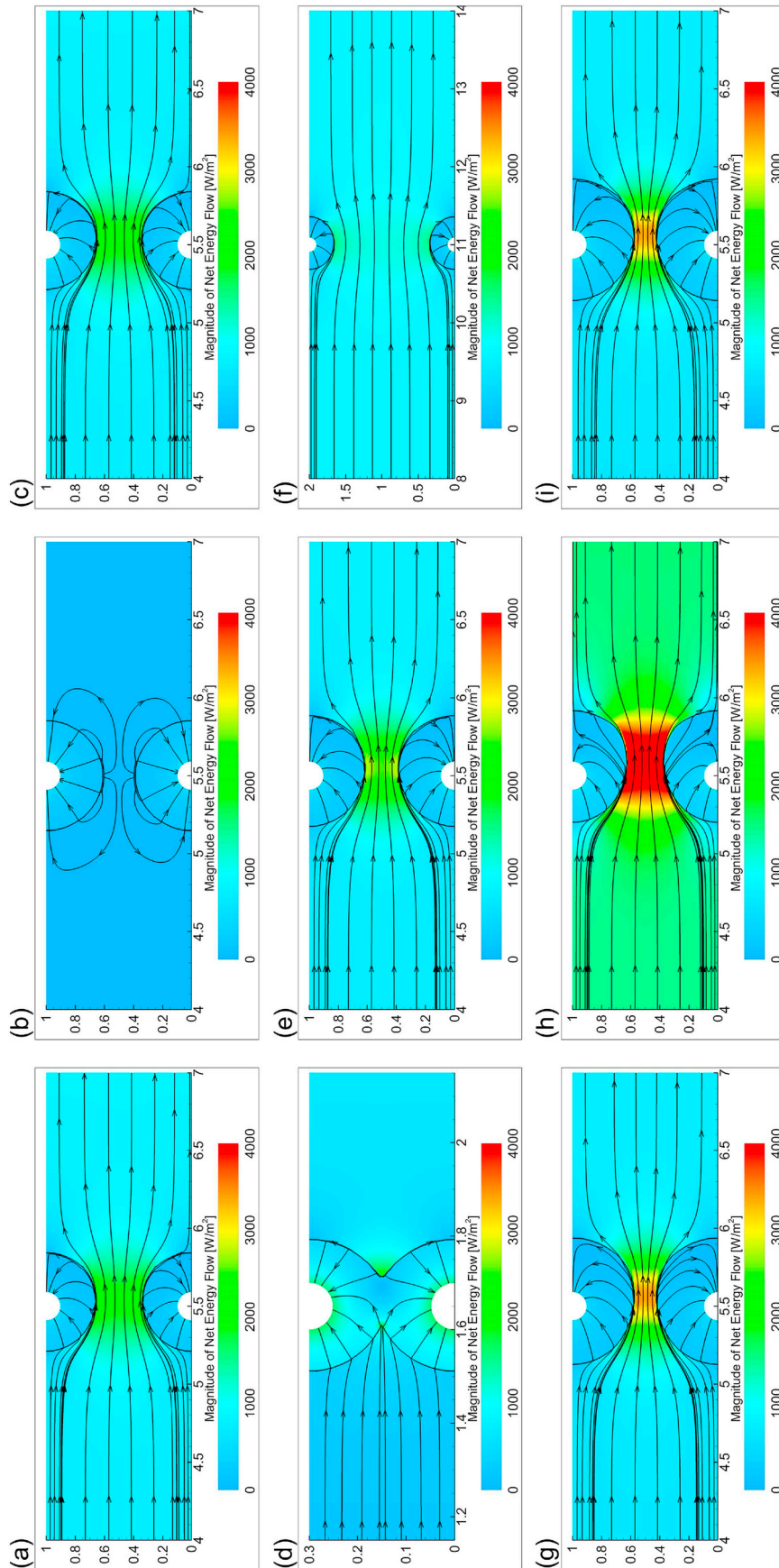


Fig. 9. The progression of the frozen body after 3 [day] of freezing under various design and operating parameters: (d), (e), and (f) highlight the effect of pipes spacing; (b), (e), and (f) highlight the effect of freeze pipes coolant's temperature; and (c), (e), and (g) display the effect of the seepage temperature. Individual plots describe certain parameter: (a) coolant's temperature of -20 [$^{\circ}\text{C}$]; (b) no-seepage condition; (c) seepage temperature of 5 [$^{\circ}\text{C}$]; (e) spacing of 1.0 [m] (base case); (f) spacing of 2.0 [m]; (g) seepage temperature of 5 [$^{\circ}\text{C}$]; (h) seepage of 0.1 [m/d]; and (i) coolant's temperature of -30 [$^{\circ}\text{C}$].

freeze pipes. Therefore, the AGF process should continue in order to create a closed, frozen wall.

Fig. 6 (m)-(p) and Fig. 7 (m)-(p) demonstrate the performance of AGF process under seepage velocity of 2 [m/day]. The overall behavior is drastically changed, as compared to the previous cases. Clearly, high seepage velocity hinders the hydraulic sealing between the freeze pipes. The energy of the freeze pipes is not powerful enough to overcome the high-velocity of the warm groundwater seepage, which could have a significant impact on the overall AGF process. Also, by comparing the magnitude of the net energy flow in the unfrozen areas throughout the freezing process, one can observe a minimal change in the overall magnitude. However, in the previous two cases (1 and 1.4 [m/day]), the magnitude reduced significantly from its initial values. This means that at high seepage velocity of 2 [m/day] the convective and conductive parts of the energy flow, as described in Eq. (11), reach an equilibrium stage, where the power of the heat sinks is not adequate to advance the size of the frozen body.

5.2. Spacing between freeze pipes

The distance between freeze pipes is one of the main design parameters in any AGF system, which requires particular attention during the design stage. In this study, three typical freeze pipes' spacing in underground mines were selected (see Table 2). Fig. 8 (d), (e), and (f) reveals the effect of the distance between two freeze pipes on the development of the frozen body. The x-axis and y-axis are the lengths in meters. The figures show the temperature contours and the velocity streamlines of each case after three days of continuous freezing. The radius of the frozen body reduces while spacing between two pipes increases. This is to be expected for two reasons: (i) the fact of having two heat sinks (i.e., the freeze pipes), and (ii) the size of the ground structure that needs to be frozen, which is characterized by the distance between the pipes. If a freezing system has a single freeze pipe, one can predict a similar growth rate under similar operating conditions. In our case, however, there are two freeze pipes. The contribution of the neighbor freeze pipe to the growth of the frozen body is inversely proportional to the distance between the pipes at the same time frame.

The corresponding heatlines are observed in Fig. 9(d) and (e), and (f). The heatlines of the 0.3 [m] case, as indicated in Fig. 9 (d), are pointed directly to the freeze pipes, showing that the groundwater seepage has a negligible effect on the progression of the frozen wall. As defined in Eqn. (11), the conductive part of the net energy flow is inversely proportional to the characteristic length, L , of the medium ($q \propto 1/L$). This leads us to the fact that at the same operating conditions, the contribution of the conductive heat transfer to the net energy flow reduces with increasing the distance between the freeze pipes.

5.3. Velocity of the groundwater seepage

The groundwater seepage is one of the main challenges that face any AGF process. It increases the time needed to create a closed, frozen wall. In certain conditions, the flow could prevent the hydraulic sealing between two freeze pipes. Fig. 8 (b), (e), and (h) and Fig. 9 (b), (e), and (h) demonstrate the impact of the groundwater seepage on the evolution of the frozen body after three days of continuous freezing. Clearly, the thickness of the frozen wall is identical in the three cases. The elongation in the flow direction, however, is greater at higher seepage velocity. While discussing the seepage velocity and the growth of the frozen wall, it is instructive to introduce here the Péclet number, which is a dimensionless number that is used in calculations involving convective heat transfer.

$$Pe = \frac{\text{heat transport by convection}}{\text{heat transport by conduction}} = \frac{uL}{\alpha} \quad (17)$$

where ($\alpha = k/(\rho c_p)$) is the thermal diffusivity. Based on the definition of the Péclet number, Pe , and the formulation of the energy flow in Eq.

(11), one can anticipate that, at the same operating conditions, increasing the seepage velocity will boost the heat transport by convection, as compared to the heat transport by conduction, which in turn increases the magnitude of the net energy flow in the unfrozen area. Thus, affecting the growth and the shape of the frozen body by dragging some heatlines away from the freeze pipes, which can be observed in Fig. 9 (e) and (h).

5.4. Temperature of the coolant

The temperature of the coolant is one of the key operating parameters that determine the thickness of the frozen body. The sub-zero temperature is required to overcome the sensible and latent heat of the groundwater in the porous ground structure. In this study, three brine's temperatures are analyzed: -20 , -25 , and -30 [°C]. The results of these three cases are shown in the diagonal plots in Fig. 8 (a), (e), and (i) and Fig. 9 (a), (e), and (i). Several features are apparent in these plots, notably that the frozen body gets thicker when wall's temperature is colder. The dominating mechanism in the frozen area is conduction. The conductive heat transfer, q , has a proportional relationship with the temperature difference, $q \propto \Delta T$. Thus, at lower brine's temperature, the frozen body should be thicker, taking into consideration similar design and operating conditions. Moreover, because the frozen body is thicker at lower coolant's temperature, the free aisle between the frozen areas is narrower. Thus, the seepage velocity increases, as illustrated previously, forcing the frozen body to prolong in the direction of the flow.

5.5. Temperature of the seepage

The temperature of the groundwater flow has the least effect on the thickness and the shape of the frozen body, as compared to the other parameters, as depicted in Fig. 8 (c), (e), and (g) and Fig. 9 (c), (e), and (g). Note, however, that the frozen body at seepage temperature of 5 [°C] is somewhat thicker than the frozen wall at 15 [°C], as inferred from Fig. 8 (g) and (c), respectively. This behavior can be attributed to the enthalpy of the seepage, which is directly related to the flow temperature; ($dh = c_p dT$). At higher enthalpy, the freeze pipes require more energy to overcome convective energy of the warm flow. The physical reasoning behind the stretch of the frozen body in the direction of the flow is similar to the previous discussion.

5.6. Closure time

Thus far, we have examined the impact of design and operating parameters on the progression of the frozen body, and now we address the effect of the parameters on the closure time, which is defined as the time needed to create a closed, frozen wall between two freeze pipes with a core temperature of -5 [°C].

Fig. 10(a) shows the closure time at different spacing. At 0.3 [m] spacing, the closure time is around 2.2 [day]. The symmetrical freezing growth of this case, as inferred in Fig. 11(d), shows that the groundwater seepage has a negligible effect on the AGF process when the freeze pipes are close to each other. At 1.0 [m] spacing, the time increases to a value around 9.1 [day]; 4.5 times higher than the 0.3 [m] case. The closure time increases substantially to 72.1 [day] at 2.0 [m] spacing. This increase is due to the fact that the ground domain per pipe's unit length increases dramatically, while the heat sink in all cases stay the same: two freeze pipes with coolant temperature of -25 [°C]. The domain size per pipe's unit length increases from (0.3 [m] \times 3.3 [m]), (1.0 [m] \times 11.0 [m]), to (2.0 [m] \times 22.0 [m]). The width of the domain increases to satisfy the boundary-condition independence that has been discussed previously. Even if the ground domain has the same width of 3.3 [m], still, the size of the domain increases from 1 [m³], to 3.3 [m³], and to 6.6 [m³]. Hence, higher sensible and latent energy, and higher convective flux associated with the 10 [°C] groundwater flow have to be extracted by the same freeze pipes. Thus, the closure time

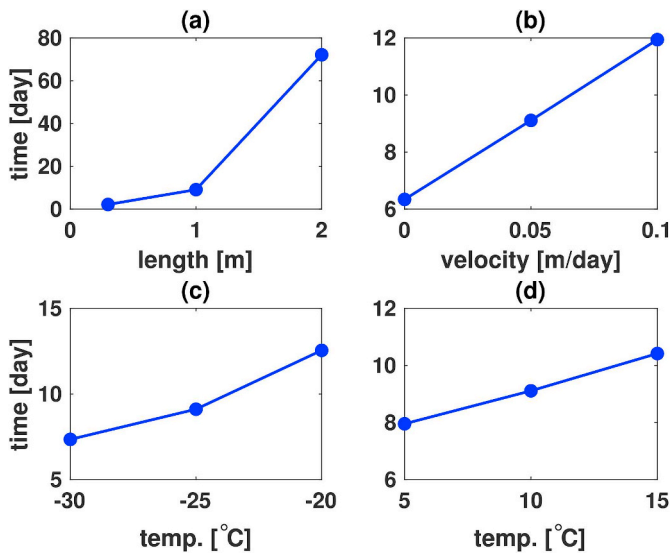


Fig. 10. The influence of the freeze pipes' spacing, seepage velocity, freeze pipe coolant's temperature, and seepage temperature on the closure time.

increases substantially with freeze pipes spacing.

Furthermore, the downstream part of the frozen body tends to elongate in the direction of the seepage. Ideally, a single freeze pipe creates a circular frozen body. However, the warm groundwater seepage forces the frozen body to lengthen in the same direction of the flow. The elongation has a proportional relation with the spacing, as shown in Fig. 11(e) and (f). As discussed previously, the freeze pipes require more time to create a closed, frozen body when the spacing is larger; hence the seepage has more influence on the shape of the frozen body at 2.0 [m] spacing, as compared to 0.3 [m] case.

In the case of no-seepage, the time needed to create a closed body is

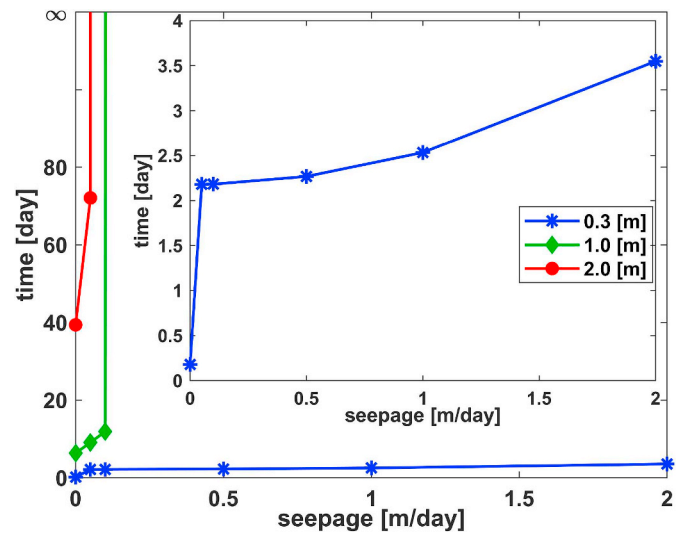


Fig. 12. The effect of the groundwater seepage on the closure time at different freeze pipes' spacing; 0.3, 1.0, and 2.0 [m].

around 6.4 [day], as shown in Fig. 10 (b). The main heat sink is the freeze pipes. Therefore, the shape of the frozen body is symmetrical in x and y directions, as shown in Fig. 11 (b). In the case of 0.05 [m/d] seepage, it took the freeze pipes 9.1 [day] to create the required frozen body. One can observe from Fig. 11 (e) that the frozen body is slightly shifted in the direction of the flow. However, the heat flux through the freeze pipes is large enough to overcome the energy of the flow. Now, in the case of 0.1 [m/d] the freeze pipes require more energy to overcome the total energy of the flow. The closure time, in this case, increases to almost 12 [days]. It is notable here that the width of the downstream part of the frozen body increases from 0.5 [m] at the no-seepage scenario, to 1 [m] in the highest velocity case (see Fig. 11(e) and (f)). This

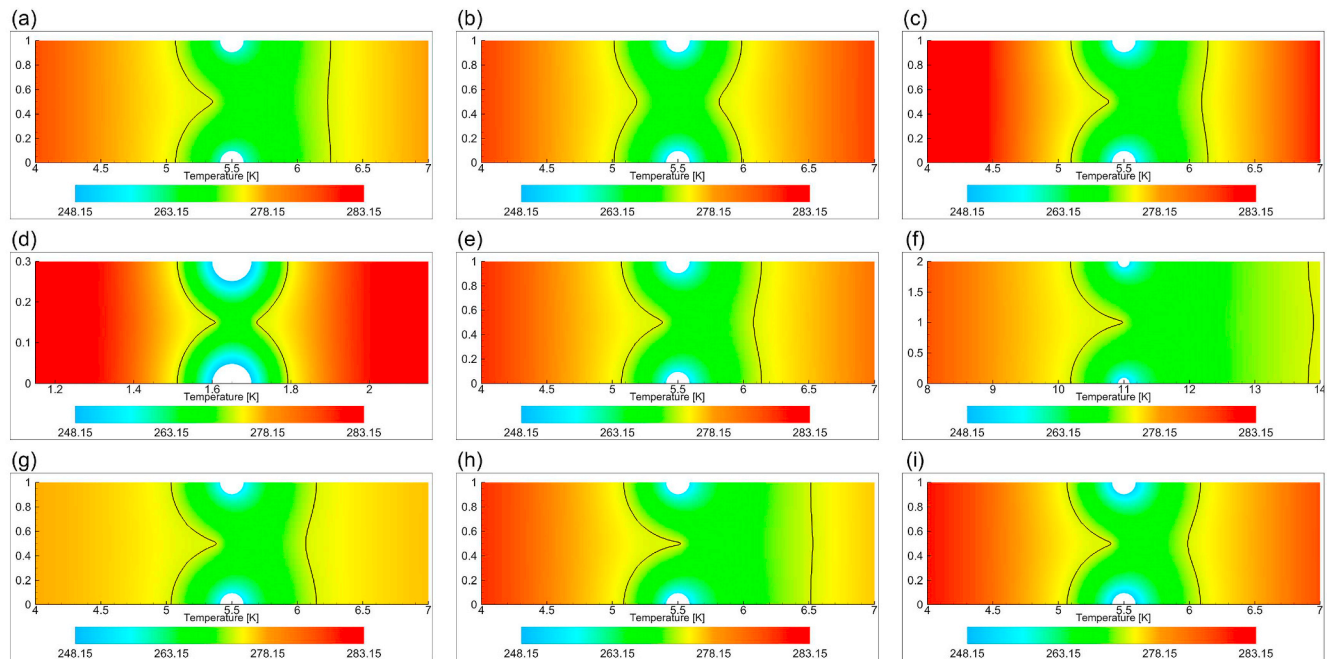


Fig. 11. Temperature contours of AGF process at different design and operating conditions. The frozen bodies are represented here with the zero iso-therm. horizontal plots (d), (e), and (f) highlight the effect of pipes spacing; vertical plots (b), (e), and (h) represent the impact of groundwater seepage; the other diagonal plots (c), (e), and (g) display the effect of the seepage temperature. Individual plots describe certain parameter: (a) coolant's temperature of -20 [°C]; (b) no-seepage condition; (c) seepage temperature of 15 [°C]; (d) spacing of 0.3 [m]; (e) spacing of 1.0 [m] (base case); (f) spacing of 2.0 [m]; (g) seepage temperature of 5 [°C]; (h) seepage of 0.1 [m/d]; and (i) coolant's temperature of -30 [°C].

is due to the higher convective energy of the flow.

Before addressing the effect of coolants' and seepage's temperatures, we return our attention to the interaction between groundwater seepage and freeze pipes' spacing with a view to the impact on the closure time. Fig. 12 demonstrates the influence of groundwater seepage on the closure time at different pipes' spacings. One can observe that the closure time at 0.3 [m] spacing is way shorter than the other two cases, in spite of the existence of the seepage. Moreover, the closure time jumped suddenly from around 4.5 [hr], with no-seepage, to around 2 [day], although the seepage velocity is as low as 0.01 [m/day]. This demeanor emphasizes the significant impact and the important role of the groundwater seepage on the formation of the frozen wall. On the other hand, at the pipes' spacing of 1 and 2 [m], it is observed from the figure that the seepage hinders the formation of a closed, frozen wall at velocities higher than 0.1 and 0.05 [m/day], respectively. These results highlight the importance of developing proper design parameter prior to actual construction takes place.

Fig. 10(c) shows the influence of the coolant's temperature on the closure time. At brine's temperature of -30 [°C], the freeze pipes require 7.4 [day] to create a frozen wall. The time increases to 9.1 and 12.6 [day] while coolant's temperature increases to -25 and -20 [°C], respectively. This is to be expected since the brine's temperature is directly and proportionally related to the heat flux through the freeze pipes. Lower coolant's temperature means higher ΔT between the pipe and the ground, which yields a higher heat transfer rate. Consequently, less time is required to overcome the ground's and seepage's energy. Fig. 11 (a), (e), and (i) illustrate the effect of the brine's temperature on the thickness and shape of the frozen body. Although the total width of the frozen body in the coldest freeze pipe case is the lowest, which is in certain cases undesirable, the time needed to reach this stage is less than the time in the coolant's temperature of -20 [°C] case. Therefore, at the same time t , the width of the coldest freeze pipes at -30 [°C] will be larger than the width at -20 [°C] brine's temperature case.

The seepage temperature has the smallest impact on the closure time, as compared to the other parameters. The closure time increases from 8 [day] at flow temperature of 5 [°C] to 9.1 [day] and to 12 [day] in the case of flow at 10 [°C] and 15 [°C], respectively, which can be discerned from Fig. 10 (d). Also, the change of the frozen body width and shape is negligible as compared to the other cases, as inferred in Fig. 11 (c), (e), and (g). The discussion of the effect of this parameter on the AGF process has been illustrated previously in Section 5.5.

6. Conclusions

A mathematical model of an artificial ground freezing process under various seepage velocity has been derived, analyzed, and validated. A computational study, has been carried out with a view to studying how various design and operating parameters affect the overall performance of the AGF process. The concept of heatlines has been introduced to provide a deeper understanding of the impact of the groundwater seepage along with other design and operating parameters on the development of the frozen body between two freeze pipes.

It has been shown that a range of parameters - freeze pipes' spacing, seepage velocity, coolant's temperature, and seepage temperature - affect the overall performance of the AGF process in terms of closure time, frozen body thickness, and shape of the frozen wall. It should also be mentioned that the spacing between two freeze pipes has the highest influence on the freezing time and the shape of the frozen body. On the contrary, the seepage temperature has the least influence among the other parameters on the performance of AGF process.

The computational study presented here can be extended to, e.g., optimize the design and operating condition based on the analysis of the heatlines and the entropy generation, which will be our future work.

Conflicts of interest

The authors declared that there is no conflict of interest.

Acknowledgements

The authors thank the Ultra Deep Mining Network (UDMN) (241695 Tri-Council (NCE UDMN) 2-003), Cameco Corporation, Newmans Geotechnique Inc., and Orano Canada Inc. (previously Areva Resources Canada Inc.). The simulations were conducted at McGill HPC facility under Calcul-Quebec and Compute-Canada with contribution from CFI-JELF. The first author gratefully acknowledged McGill Engineering Doctoral Award (MEDA) and Fonds de recherche du Québec - Nature et technologies (FRQNT) - Bourses de doctorat (B2X) for supporting this research.

References

- [1] M. Vitel, A. Rouabhi, M. Tijani, F. Guérin, Thermo-hydraulic modeling of artificial ground freezing: application to an underground mine in fractured sandstone, *Comput Geotech* 75 (2016) 80–92.
- [2] Y. Kang, Q. Liu, Y. Cheng, X. Liu, Combined freeze-sealing and new tubular roof construction methods for seaside urban tunnel in soft ground, *Tunn Undergr Space Technol* 58 (2016) 1–10.
- [3] E. Pimentel, S. Papakonstantinou, G. Anagnostou, Numerical interpretation of temperature distributions from three ground freezing applications in urban tunnelling, *Tunn Undergr Space Technol* 28 (2012) 57–69.
- [4] S. Amuno, A. Jamwal, B. Grahn, S. Niyogi, Chronic arsenicosis and cadmium exposure in wild snowshoe hares (*Lepus americanus*) breeding near yellowknife, northwest territories (Canada), part 1: evaluation of oxidative stress, antioxidant activities and hepatic damage, *Sci Total Environ* 618 (2018) 916–926.
- [5] I.K. Iskandar, Effect of freezing on the level of contaminants in uncontrolled hazardous waste sites. part 1. literature review, *Cold Reg Res Eng Lab* 86 (19) (1986) 1–33.
- [6] I.K. Iskandar, Ground freezing controls hazardous waste, *Mil Eng* 79 (1987) 455–456.
- [7] M.A. Alzoubi, A. Nie-Rouquette, A.P. Sasmito, Conjugate heat transfer in artificial ground freezing using enthalpy-porosity method: experiments and model validation, *Int J Heat Mass Transf* 126 (2018) 740–752.
- [8] F. Sanger, F. Sayles, Thermal and rheological computations for artificially frozen ground construction, *Eng Geol* 13 (1–4) (1979) 311–337.
- [9] X. Hu, Z. Hong, T. Fang, Analytical solution to steady-state temperature field with typical freezing tube layout employed in freeze-sealing pipe roof method, *Tunn Undergr Space Technol* 79 (2018) 336–345.
- [10] X.-d. Hu, T. Fang, Y.-g. Han, Mathematical solution of steady-state temperature field of circular frozen wall by single-circle-piped freezing, *Cold Reg Sci Technol* 148 (2018) 96–103.
- [11] X.-d. Hu, T. Fang, L.-y. Zhang, Analytical solution to temperature distribution in frozen soil wall with wavy boundaries by single-row-and double-row-piped freezing, *Cold Reg Sci Technol* 145 (2018) 208–228.
- [12] T. Li, Y. Zhou, X.-y. Shi, X.-x. Hu, G.-q. Zhou, Analytical solution for the soil freezing process induced by an infinite line sink, *Int J Therm Sci* 127 (2018) 232–241.
- [13] A.C. Fowler, W.B. Krantz, A generalized secondary frost heave model, *SIAM J Appl Math* 54 (6) (1994) 1650–1675.
- [14] S. Huang, Y. Guo, Y. Liu, L. Ke, G. Liu, et al., Study on the influence of water flow on temperature around freeze pipes and its distribution optimization during artificial ground freezing, *Appl Therm Eng* 135 (2018) 435–445.
- [15] K. Hansson, J. Simunek, M. Mizoguchi, L.-C. Lundin, M.T. Van Genuchten, Water flow and heat transport in frozen soil, *Vadose Zone J* 3 (2) (2004) 693–704.
- [16] J.M. McKenzie, C.I. Voss, D.I. Siegel, Groundwater flow with energy transport and water-ice phase change: numerical simulations, benchmarks, and application to freezing in peat bogs, *Adv Water Resour* 30 (4) (2007) 966–983.
- [17] W. Yu, W. Liu, Y. Lai, L. Chen, X. Yi, Nonlinear analysis of coupled temperature-seepage problem of warm oil pipe in permafrost regions of northeast China, *Appl Therm Eng* 70 (1) (2014) 988–995.
- [18] W. Song, Y. Zhang, B. Li, X. Fan, A lattice Boltzmann model for heat and mass transfer phenomena with phase transformations in unsaturated soil during freezing process, *Int J Heat Mass Transf* 94 (2016) 29–38.
- [19] A. Marwan, M.-M. Zhou, M.Z. Abdelrehim, G. Meschke, Optimization of artificial ground freezing in tunneling in the presence of seepage flow, *Comput Geotech* 75 (2016) 112–125.
- [20] M. Vitel, A. Rouabhi, M. Tijani, F. Guérin, Modeling heat and mass transfer during ground freezing subjected to high seepage velocities, *Comput Geotech* 73 (2016) 1–15.
- [21] A. Brent, V. Voller, K. Reid, Enthalpy-porosity technique for modeling convection-diffusion phase change: application to the melting of a pure metal, *Numer Heat Trans Part A Appl* 13 (3) (1988) 297–318.
- [22] M. Jourabian, M. Farhadi, A.R. Darzi, Constrained ice melting around one cylinder in horizontal cavity accelerated using three heat transfer enhancement techniques, *Int J Therm Sci* 125 (2018) 231–247.

- [23] V.R. Voller, C. Prakash, A fixed grid numerical modelling methodology for convection-diffusion mushy region phase-change problems, *Int J Heat Mass Transf* 30 (8) (1987) 1709–1719.
- [24] A. König-Haagen, E. Franquet, E. Pernot, D. Brüggemann, A comprehensive benchmark of fixed-grid methods for the modeling of melting, *Int J Therm Sci* 118 (2017) 69–103.
- [25] S. Kimura, A. Bejan, The heatline visualization of convective heat transfer, *J Heat Tran* 105 (4) (1983) 916–919.
- [26] P.S. Mahapatra, A. Mukhopadhyay, N.K. Manna, K. Ghosh, Heatlines and other visualization techniques for confined heat transfer systems, *Int J Heat Mass Transf* 118 (2018) 1069–1079.
- [27] M. Al-Jethelah, S.H. Tasnim, S. Mahmud, A. Dutta, Melting of nano-pcm in an enclosed space: scale analysis and heatline tracking, *Int J Heat Mass Transf* 119 (2018) 841–859.
- [28] T.P. Lima, M.M. Ganzarolli, A heatline approach on the analysis of the heat transfer enhancement in a square enclosure with an internal conducting solid body, *Int J Therm Sci* 105 (2016) 45–56.
- [29] M.A. Alzoubi, A.P. Sasmito, A. Madiseh, F.P. Hassani, Intermittent freezing concept for energy saving in artificial ground freezing systems, *Energy Procedia* 142 (2017) 3920–3925.
- [30] M. Vitel, A. Rouabhi, M. Tijani, F. Guérin, Modeling heat transfer between a freeze pipe and the surrounding ground during artificial ground freezing activities, *Comput Geotech* 63 (2015) 99–111.
- [31] E. Pimentel, A. Sres, G. Anagnostou, Modelling of ground freezing in tunnelling, *Underground Space-The 4th Dimension of Metropolises*, ITA and World Tunnel Congress, Prague, 2007, pp. 331–336.
- [32] E. Pimentel, A. Sres, G. Anagnostou, Large-scale laboratory tests on artificial ground freezing under seepage-flow conditions, *Geotechnique* 62 (3) (2012) 227.
- [33] M. Kaviany, *Principles of Heat Transfer in Porous Media*, Springer, 1995.
- [34] T. Tang, J. McDonough, A theoretical model for the porosity–permeability relationship, *Int J Heat Mass Transf* 103 (2016) 984–996.
- [35] C. Beckermann, R. Viskanta, Natural convection solid/liquid phase change in porous media, *Int J Heat Mass Transf* 31 (1) (1988) 35–46.
- [36] J. Happel, H. Brenner, *Low Reynolds Number Hydrodynamics: with Special Applications to Particulate Media* vol. 1, Springer Science & Business Media, 2012.
- [37] N. Zhang, Z. Wang, Review of soil thermal conductivity and predictive models, *Int J Therm Sci* 117 (2017) 172–183.
- [38] V. Voller, C. Swaminathan, General source-based method for solidification phase change, *Numer Heat Tran, Part B Fundamentals* 19 (2) (1991) 175–189.
- [39] A.M. Morega, A. Bejan, Heatline visualization of forced convection laminar boundary layers, *Int J Heat Mass Transf* 36 (16) (1993) 3957–3966.
- [40] A. Sres, *Theoretische und experimentelle Untersuchungen zur künstlichen Bodenvereisung im strömenden Grundwasser* vol. 18378, vdf Hochschulverlag AG, 2010.
- [41] V. Voller, C. Swaminathan, B.G. Thomas, Fixed grid techniques for phase change problems: a review, *Int J Numer Methods Eng* 30 (4) (1990) 875–898.